

EXPERIMENTAL VALIDATION OF THE POTENTIAL FIELD LANEKEEPING SYSTEM

E. J. ROSSETTER, J. P. SWITKES* and J. C. GERDES

Design Division Terman 551, Mechanical Engineering, Stanford University, Stanford, CA 94305

(Received 15 August 2003; Revised 25 January 2004)

ABSTRACT—Lanekeeping assistance has the potential to save thousands of lives every year by preventing accidental road departure. This paper presents experimental validation of a potential field lanekeeping assistance system with quantitative performance guarantees. The lanekeeping system is implemented on a 1997 Corvette modified for steer-by-wire capability. With no mechanical connection between the hand wheel and road wheels the lanekeeping system can add steering inputs independently from the driver. Implementation of the lanekeeping system uses a novel combination of a multi-antenna Global Positioning System (GPS) and precision road maps. Preliminary experimental data shows that this control scheme performs extremely well for driver assistance and closely matches simulation results, verifying previous theoretical guarantees for safety. These results also motivate future work which will focus on interaction with the driver.

KEY WORDS : Lanekeeping, Driver assistance, GPS/INS, Potential field, Vehicle dynamics, DGPS, Road mapping

NOMENCLATURE

(D)GPS : (differential) global positioning system
INS : inertial navigation sensor
DOF : degree(s) of freedom
PD : proportional derivative
CEP : circular error precision
Hz : hertz (cycles per second)
xPC : xPC operating system
VSBC : versalogic single board computer
CG : center of gravity
PPS : pulse per second time reference

1. INTRODUCTION

The design of active safety systems for today's complex driving environment may seem to be a daunting task. Active assistance systems can not address every potentially hazardous situation a vehicle may encounter. However, a surprisingly large number of vehicle fatalities occur simply from lane departures. In 2001 43% of all vehicle fatalities were caused by collision with a fixed obstacle, accounting for over 18,000 deaths (NHTSA, 2002). Recent advances in sensing, computing, and actuation make active lanekeeping assistance possible and feasible for production in the very near future. By simply helping the driver remain in the lane, such

systems can save thousands of lives every year.

Lanekeeping assistance is an active area of research in industry and academic research institutions. One big question in the design of active lanekeeping systems is how to best integrate the driver with the active controller. Ideally, this should be done in a way that provides a guarantee of lanekeeping ability in the absence of adequate steering commands from the driver, while remaining unobtrusive during normal driving. The conflicting nature of these two goals was noted by Fujioka *et al.* (1999) who developed a system that used the input from the driver along with the command from a 'virtual' driver to determine the total steering command. Testing on a fixed based driving simulator revealed that the driver acceptance of this approach was inversely related to the 'virtual' driver's influence. Another approach to actively assist the driver was proposed by Leblanc (1996) who used differential braking to add corrective moments to aid in lanekeeping. In contrast to Fujioka's approach this method addresses the competing influences of the driver and controller by leaving the driver in control of the steering command. Although work in this area has addressed important issues in the design of active lanekeeping systems it has not provided a quantitative way to guarantee the lanekeeping ability of the vehicle.

To create a system that works cooperatively with the driver and provides analytical bounds on the vehicle motion, Gerdes and Rossetter (2001) proposed a method for lanekeeping assistance using the paradigm of artificial

*Corresponding author. e-mail: switkesj@stanford.edu

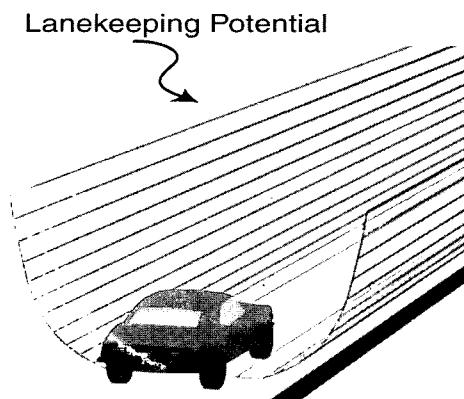


Figure 1. Potential field for lanekeeping.

potential fields. In this work, control forces are derived from an ‘artificial’ potential function to aid the driver in avoiding environmental obstacles. The potential function is an intuitive approach to representing levels of hazard. The potential’s peaks correspond to large hazards while safe regions of the road are represented by low or zero potential function values. An exaggerated example of a lanekeeping potential is depicted in Figure 1. The actual size of a potential necessary for highway lanekeeping would be about the size of a typical road crown for drainage (a few centimeters), but inverted to have a minimum at lane center. When the vehicle moves towards the lane edge, control forces derived from the potential nudge the vehicle towards safer regions of the road. Since this control scheme is designed for driver assistance it does not cancel or alter the handling characteristics of the vehicle. As a result, the vehicle dynamics presented to the driver remain consistent and predictable.

By utilizing the inherent system damping it is possible to mathematically bound the lateral motion of the vehicle in the presence of time-varying disturbances, providing a safety guarantee for the lanekeeping assistance system (Rossetter, 2003). The potential field approach provides a compact mathematical framework for lanekeeping assistance based on simple vehicle models. Experimental validation is necessary to confirm the performance of this approach in the presence of unmodeled dynamics, sensor noise, and actuator limitations. This paper presents a novel approach to implementing this lanekeeping system and experimental results that verify the mathematical lanekeeping bounds provided by the potential field framework.

Implementing this lanekeeping system requires actuation and sensing which are not currently available on production vehicles. The ability to steer the vehicle from a computer command is necessary as is highly accurate knowledge of vehicle position and heading relative to the road lane. Steering the vehicle can be accomplished

through steer-by-wire, in which the orientation of the road wheels is determined by an electronic actuator instead of a mechanical steering column. The position estimate must have an accuracy of much less than a lane width, and a sufficiently fast update for vehicle control. Many solutions to this sensing need have been proposed. Vision systems have been used by researchers such as Cerone (2002) and Gehrig (2002), who each demonstrated its use for highway lanekeeping. Magnetometers sensing magnets embedded in the road have been successfully demonstrated by researchers at PATH including Tan *et al.* (2002) for automated buses, as well as by Peng and Tomizuka (1993) for automated highways.

The system described in this paper uses a multi-antenna GPS system for determining heading and position. This setup is an attractive approach for lanekeeping assistance because it does not rely on roadway infrastructure such as magnets or lane markings, and provides accurate position estimates as well as vehicle heading that is not corrupted by vehicle sideslip. GPS is freely accessible and public efforts for nationwide differential corrections are currently underway (USCG, 2003). GPS does have some limitations for vehicle safety systems such as loss of the GPS signal due to obstruction and errors due to multi-path or atmospheric disturbances. While integration of the GPS with inertial sensors can mitigate these problems, a production lanekeeping system would likely combine GPS with other sensing systems for robustness. GPS provides the vehicle’s global position and heading but for lanekeeping the vehicle’s position and heading relative to the lane center is needed. In this work, the relation of the vehicle to the road is determined by comparing the vehicle’s heading and position to an accurate digital map that represents the desired vehicle location. The mapping scheme used in this work is different from techniques used by others for GPS based lanekeeping because it uses continuous curves to represent the road as opposed to straight segments (Rogers, 2000) or interpolation between data points (Omae, 1999). The multi-antenna GPS configuration combined with inertial sensors provides smooth estimates of vehicle position and heading. These estimates combined with this mapping technique result in accurate lanekeeping with comfortable and smooth vehicle motion.

This paper gives a brief introduction to the potential field approach and the mathematical bounds for the lateral motion of the vehicle. This is followed by a detailed description of the key components used in the implementation of this system. This includes a novel use of a multi-antenna GPS system, the Kalman filters used to estimate vehicle position and heading, and the creation of the digital maps. The vehicle used for the testing is a 1997 C5 Corvette modified to incorporate steer-by-wire. The experimental results obtained show that the system

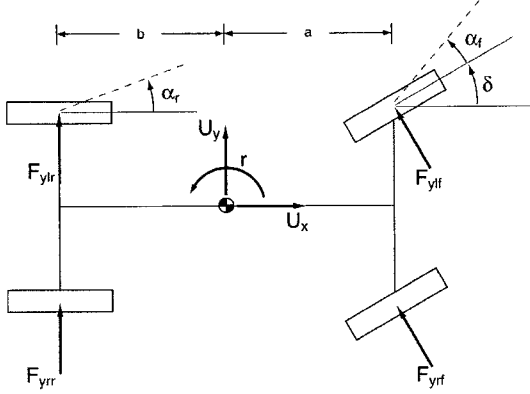


Figure 2. Vehicle model.

can keep the vehicle from leaving the lane in the absence of driver inputs. The experimental data matches remarkably well with simulation of the simple vehicle dynamics used in the theoretical development of the potential field framework. This predictability through simulation is extremely encouraging because it verifies that the mathematical bounds for the lateral motion of the vehicle work well in practice, providing a safety guarantee for the lanekeeping system.

2. VEHICLE DYNAMICS

The development of this controller uses a 3-DOF bicycle model as shown in Figure 2. The equations of motion are

$$m\dot{U}_x = F_{xr} + F_{xf} \cos \delta - F_{yf} \sin \delta + mrU_y \quad (1)$$

$$m\dot{U}_y = F_{yr} + F_{yf} \sin \delta - F_{xf} \cos \delta - mrU_x \quad (2)$$

$$I_z \dot{r} = aF_{xf} \sin \delta + aF_{yf} \cos \delta - bF_{yr} \quad (3)$$

where

$$F_{xf} = F_{xrf} + F_{xlf} \quad (4)$$

$$F_{xr} = F_{xrr} + F_{xlr} \quad (5)$$

$$F_{yf} = F_{yrf} + F_{ylf} \quad (6)$$

$$F_{yr} = F_{yrr} + F_{yrl} \quad (7)$$

Assuming equal slip angles on the left and right wheels, the front and rear slip angles are

$$\alpha_f = \tan^{-1} \left(\frac{U_y + ra}{U_x} \right) - \delta \quad (8)$$

$$\alpha_r = \tan^{-1} \left(\frac{U_y - rb}{U_x} \right) \quad (9)$$

Using a linear tire model, the lateral forces are given as

$$F_{yf} = -C_f \alpha_f \quad (10)$$

$$F_{yr} = -C_r \alpha_r \quad (11)$$

where C_f and C_r are the front and rear cornering stiffnesses, respectively. Substituting the expressions for the lateral forces into Equations (1) through (3) and making a small angle approximation for the steering and slip angles yields

$$m\dot{U}_x = mrU_y + F_{xr} + F_{xf} \quad (12)$$

$$m\dot{U}_y = -C_r \left(\frac{U_y - rb}{U_x} \right) - C_f \left(\frac{U_y + ra}{U_x} \right) - mrU_x + C_f \delta + F_{xf} \delta \quad (13)$$

$$I_z \dot{r} = aF_{xf} \delta - aC_f \left(\frac{U_y + ra}{U_x} \right) + bC_r \left(\frac{U_y - rb}{U_x} \right) + aC_f \delta \quad (14)$$

The dynamics include components that are directly controlled by the steering angle and longitudinal forces as well as drift terms that only depend on vehicle states. It is convenient to separate the dynamics into the drift terms and controlled terms as follows:

$$M\ddot{q} = f(\dot{q}) + g(q, u_c) \quad (15)$$

where $q = [U_x \ U_y \ r]^T$ and the control vector $u_c = [\delta \ F_{xf} \ F_{xr}]^T$. M is the mass matrix, $f(\dot{q})$ contains the terms that are not influenced by the control vector and $g(u_c)$ has the remaining controlled terms.

$$M = \begin{bmatrix} m & 0 & 0 \\ 0 & m & 0 \\ 0 & 0 & I_z \end{bmatrix} \quad (16)$$

$$f(\dot{q}) = \begin{bmatrix} mrU_y \\ -C_r \left(\frac{U_y - rb}{U_x} \right) - C_f \left(\frac{U_y + ra}{U_x} \right) - mrU_x \\ -aC_f \left(\frac{U_y + ra}{U_x} \right) + bC_r \left(\frac{U_y - rb}{U_x} \right) \end{bmatrix} \quad (17)$$

$$g(u_c) = \begin{bmatrix} F_{xr} + F_{xf} \\ C_f \delta + F_{xf} \delta \\ aF_{xf} \delta + aC_f \delta \end{bmatrix} \quad (18)$$

The controlled terms, $g(u_c)$, are determined by the desired control forces as described in the following section. Once the values of the controlled terms are known, it is possible to solve for the control vector, u_c (Gerdes, 2000).

3. LANEKEEPING CONTROLLER

The control law introduced by Gerdes and Rossetter (2001) applies a control force to the vehicle derived from the gradient of an artificial potential function. This control approach is closely related to previous work in robotics (e.g. Khatib, 1986; Hogan, 1985) with the objective being

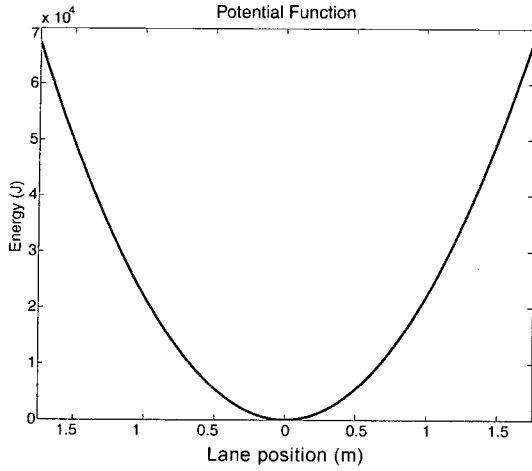


Figure 3. Quadratic potential function.

a nominally safe driving environment as opposed to end-effector placement or trajectory generation. For lane-keeping, a simple quadratic potential is used with the minimum at the lane center, as shown in Figure 3.

Since the hazards are fixed in the environment (in this case, the lane edges) it makes sense to define the potential relative to the desired path. For high speed stability it is necessary to incorporate a projection (lookahead) into the potential function (Rossetter, 2002). As a result, the quadratic potential used to generate the desired control force is a function of this projected offset from the lane center, e_{la} as shown in Figure 4.

$$V(e_{la}) = k(e_{la})^2 = k(e + x_{la} \sin \Delta \psi)^2 \quad (19)$$

where x_{la} is the projected distance in front of the vehicle and k is the potential field gain.

Since only the steering can be controlled in the test vehicle, the driver controls the longitudinal forces using the accelerator and brake pedals as in a conventional vehicle. With the quadratic potential function described in Equation (19) the control law for steering is given by

$$g_s(\delta) = g_s(\delta_{driver}) + g_s(\delta_{pf}) = \begin{bmatrix} 0 \\ C_f \delta_{driver} \\ a C_f \delta_{driver} \end{bmatrix} - \begin{bmatrix} 0 \\ \frac{\partial V}{\partial e} \cos \psi \\ a \frac{\partial V}{\partial e} \cos \psi \end{bmatrix} \quad (20)$$

where $g_s(\delta)$ contains the controlled lateral forces resulting from a combination of the driver and potential field steering commands. It is straightforward to solve for the steering angle necessary for this force.

$$\delta = \delta_{driver} - \frac{1}{C_f} \frac{\partial V}{\partial e} \cos \psi \quad (21)$$

This steering angle, δ , is produced by the steer-by-wire

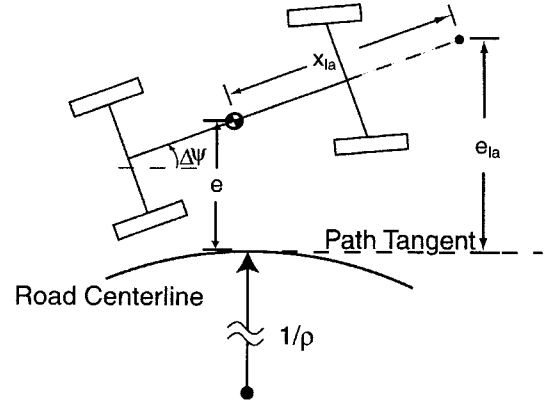


Figure 4. Global coordinates.

system described in section 5.2.

3.1. Bounding Lateral Motion

Previous work developed analytical bounds on the vehicle motion based on energy methods (Rossetter, 2003). Although the details in calculating the bounds are fairly involved the basic concept presented in this section is quite intuitive. The potential field control approach simply adds conservative forces to the existing vehicle dynamics. From an energy standpoint, this control algorithm acts as ‘artificial’ potential energy which stores the kinetic energy of the vehicle as it moves towards a lane edge. Therefore, since the vehicle dynamics can not add energy it is straightforward to show that the total system energy, defined by the kinetic energy of the vehicle and the potential energy of the controller, is non-increasing in the absence of driver inputs (Gerdes, 2001).

$$E_{total} = \frac{1}{2} m U_x^2 + \frac{1}{2} m U_y^2 + \frac{1}{2} I_z r^2 + V \quad (22)$$

$$\dot{E}_{total} \leq 0 \quad (23)$$

Since the system energy is decreasing the initial value provides a bound for the lateral motion of the vehicle by considering the worst case situation in which all the initial energy is transferred into the lanekeeping potential, V . This bound, however, can be greatly improved by creating a new energy bound that does not include the large amount of longitudinal kinetic energy in the vehicle. This makes intuitive sense for lanekeeping because the large amount of kinetic energy in the longitudinal direction should not be completely transferred into the lanekeeping potential.

To ensure that only a small amount of the vehicle's kinetic energy in the longitudinal direction is transferred into the lateral potential requires two constraints (Rossetter, 2002) on the potential field controller. The first is that the control force from the potential function must be applied in front of the neutral steer point (the

point on a vehicle where an external force creates no steady state yaw rate). This condition ensures that the vehicle rotates away from the applied control force. The control force location is determined by the coordination of the available actuators and for our test vehicle, which only uses steering for lanekeeping, the control force location is at the front axle of the vehicle and well in front of the neutral steer point. The second constraint is the choice of a specific lookahead distance in Equation (19), based on the tire cornering stiffnesses and the potential field gain.

$$x_{la} = \frac{C_f + C_r}{2k} \quad (24)$$

Using Lyapunov's direct method in combination with these two constraints, an energy-like function is formulated that consists of only the lateral and heading error directions relative to the road, e and ψ (Figure 4).

$$L = \frac{1}{2}m\dot{e}^2 + \frac{1}{2}I_z\dot{\psi}^2 + ke^2 + 2kae\psi + c_3\psi^2 \quad (25)$$

$$\dot{L} \leq 0 \quad (26)$$

where,

$$c_3 = ka(x_{la} + a) + \frac{1}{2}(aC_f - bC_r) \quad (27)$$

This Lyapunov function is a combination of the kinetic energy in the lateral and heading error directions plus a new potential energy term that accounts for the projection into the potential. Since this energy-like function does not include the longitudinal energy, it provides excellent bounds for the lateral motion of the vehicle.

Under normal driving conditions, however, vehicles are subjected to a variety of time-varying disturbances such as road curvature, side winds, and road bank angle, that can push the vehicle into the potential. To tackle this problem it is illustrative to consider the case of a constant disturbance with known magnitude such as a constant radius turn. Here the solution is fairly straight forward because the equilibrium configuration is easily found from the equations of motion. The Lyapunov function given in Equation (25) can be used for this case by redefining the function minimum to correspond with this new equilibrium point. If the disturbance is time-varying the problem becomes more difficult because the disturbance now has a frequency component. To handle this case a slight modification is needed to the structure of the Lyapunov function to capture the fact that the energy is always decreasing (due to the inherent damping) and will eventually reach the minimum of the function. This is accomplished with a small additional term related to the derivative of the potential energy.

$$L = \frac{1}{2}m\dot{e}^2 + \frac{1}{2}I_z\dot{\psi}^2 + \tilde{V} + \varepsilon\dot{\tilde{V}} \quad (28)$$

where \tilde{V} is the potential energy-like terms given in Equation (25)

$$\tilde{V} = ke^2 + 2kx_{cf}e\psi + c_3\psi^2 \quad (29)$$

and ε is a positive constant that is chosen appropriately to ensure the necessary Lyapunov conditions (Rossetter, 2003).

With this form the derivative of the Lyapunov function can be bounded by a term related to the Lyapunov function itself and a term that bounds the frequency of the disturbance.

$$\dot{\tilde{L}} \leq -\alpha\sqrt{\tilde{L}} + \kappa U_{\max} \quad (30)$$

where α is a positive constant related to the system damping, κ is related to the extra ε term added to the function, and U_{\max} is a bound placed on the frequency of the disturbance. Qualitatively, this expression shows that there is some power being put into the system related to the frequency of the disturbance while power is being removed by the inherent system damping. The magnitude of the bound on the disturbance, U_{\max} determines how far you must move until the term $-\alpha\sqrt{\tilde{L}}$ is removing the power added by the disturbance.

The last step in the bounding process is to solve this first order differential equation to obtain an exponential bound on the $\sqrt{\tilde{L}}$. This exponential bound on the Lyapunov function bounds the lateral motion of the vehicle in the presence of time-varying disturbances. Utilizing the frequency of the disturbance provides excellent bounds to the slowly-varying disturbances commonly encountered by vehicles. This technique is extremely powerful because the potential function gain can be scaled to guarantee the lanekeeping ability of the vehicle in the presence of any time-varying disturbance with only knowledge of the maximum frequency and magnitude of the disturbance.

4. CONTROL STRUCTURE FOR VEHICLE LANE-KEEPING

As shown in Equations (19)–(21), the potential field controller requires an accurate estimation of the deviation of vehicle position and heading from lane center (Figure 4). The control structure used is shown in Figure 5. Sensors include differential GPS for position and a two-antenna GPS unit for heading. These measurements are accurate but have a slow update rate, so they are combined with accelerations and yaw rate from an Inertial Measurement Unit to have an accurate estimate of state between GPS updates. A Kalman filter is used to combine the two sources of measurement and to estimate and remove bias from the inertial measurement sensor data. The Kalman filters output the vehicle's position and heading which are compared to a precision map of the

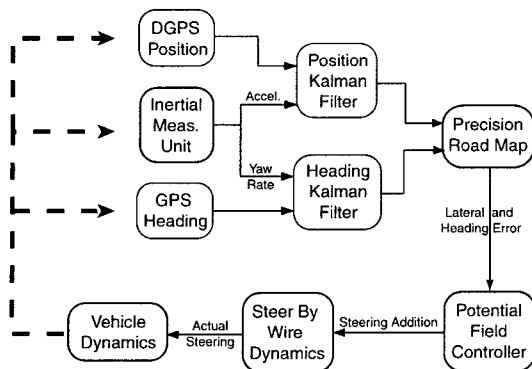


Figure 5. Control system structure.

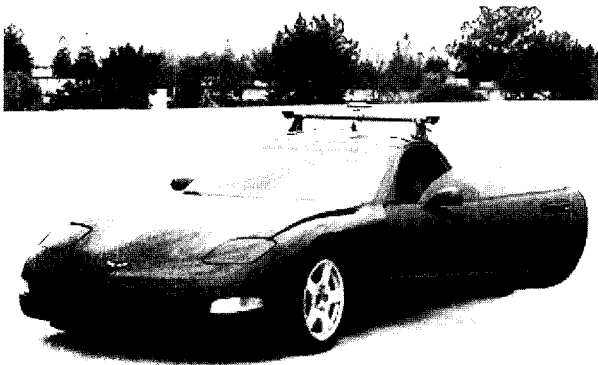


Figure 6. Steer-by-wire corvette.

road to determine the error in lateral position and heading. These errors are used by the potential field controller to calculate a steering angle (Equation 21) which is produced by the experimental steer-by-wire system.

5. SENSING AND ACTUATION

5.1. Position and Attitude Sensing

This test vehicle uses GPS to determine position and heading. GPS receivers are becoming more common on production vehicles and current applications focus on positioning information for navigation or as a locator for fast emergency response. Utilizing differential corrections and accurate maps, GPS can be combined with other sensors for lanekeeping applications. DGPS systems rely on a stationary reference receiver to cancel out most of the atmospheric error associated with ordinary GPS. The reference receiver uses its known position to calculate timing corrections to the satellite signals being received by the mobile receiver. The use of DGPS as a sensing system for autonomous vehicle control has been demonstrated by several groups. In 1992, Crow and Manning (1992) used DGPS for low speed autonomous vehicle

control. DGPS based systems were also developed and tested by Farrell and Barth (2000), Omae and Fujioka (1999) as well as Schiller *et al.* (1998). A novel multi-antenna system for attitude was combined with DGPS for low speed autonomous control of a farm tractor by Rekow *et al.* (1999). Our work combines a multi-antenna system with accurate DGPS to give independent measurements of position and heading. The heading measurement from this setup is not corrupted by vehicle sideslip and allows the estimation problem to be separated into two regular Kalman filters (described in Section 6) as opposed to using an extended Kalman filter.

For our experimental system, a carrier phase Differential Global Positioning System (DGPS) provides accurate global position information at an update rate of 10 Hz. For our test vehicle a wireless serial link is used to send the differential corrections from the reference receiver to the vehicle, once per second. With this setup, the position is accurate to a circular error precision (CEP) of 1cm. Two Novatel OEM4 GPS receiver are used: one for the reference station and one on the vehicle. The Novatel Pinwheel antenna is also used on both ends to ensure proper phasing of both GPS frequencies.

A Novatel Beeline two-antenna system is used to provide absolute vehicle heading. The system uses the difference in the relative phasing of signals between each antenna and the satellites to determine the angle of the antenna array relative to an earth fixed frame. With a 2 m baseline between the two antennae, the accuracy is about $.2^\circ$, and the update rate for the receiver is 5 Hz.

Two Bosch automotive grade inertial measurement units are used to measure lateral and longitudinal acceleration and yaw rate. Each of these units consists of an accelerometer and an angular rate gyro, with a guaranteed bandwidth of 30 Hz. These units do suffer from the bias problems associated with many inertial sensors, but these errors can be estimated and removed by combining these sensors with GPS (sec. 6).

5.2. Steer-By-Wire

The term 'steer-by-wire' refers to a steering system where the actuation of the front wheels is accomplished electronically and is completely decoupled from the drivers steering input. Steer-by-wire systems open many new horizons for automotive control including improved stability control, active handling modification, collision avoidance, and lanekeeping. Automotive manufacturers are currently developing robust steer-by-wire systems which are not currently available on production vehicles (eg. Rech, 2001; Furher, 1998; Hedenetz, 1998).

For experimental implementation of the lanekeeping system, our lab has converted a 1997 Corvette C5 to a steer-by-wire setup (Yin, 2003). This system uses a brushless DC motor to drive the input shaft of the power

steering unit. The maximum speed of the unit is approximately 39 degrees/sec at the road wheels with a bandwidth of about 2 Hz. The inputs needed for the lanekeeping task are a function of the shape of the road. For a highway situation the steering angles are less than a few degrees and the road variations are much less than 2 Hz, so the steering dynamics are not significant. Comparison of simulation with experiment (section 8) has also shown that these dynamics are negligible.

5.3. Computing

The lanekeeping controller and the steer-by-wire system is run on a Versalogic Single Board Computer (VSBC8). This machine uses a 850 MHz Pentium 3 processor, and has 128MB Ram which is used for both the operating system as well as data collection. The box has numerous 12-bit analog inputs which are used for position sensors for the steering wheel and steering shaft, as well as 16-bit analog inputs which are used for the inertial sensors. Analog outputs are used to send commands to the amplifier for the steer-by-wire motor. The box also has several serial ports, which are used to communicate with the Global Positioning receivers.

The control is programmed in Matlab Simulink, and compiled to run on the xPC operating system, a product of Mathworks. xPC is a realtime operating system with a user configurable sampling rate. Because the processor used for control is very fast, the sampling rate is not limited by computation time during each sample. The sampling rate is chosen to be at least one decade above the fastest dynamics of the system. The lateral vehicle dynamics have little content above 5 Hz, and the steering system bandwidth is about 2 Hz, so the sampling frequency is chosen to be 100 Hz.

6. KALMAN FILTERS

6.1. Overview

As shown in Figure 5, the control structure uses two Kalman filters to integrate INS sensors with GPS information for high update heading and position values. Typical GPS updates are around 10 Hz compared to the sampling rate of 100 Hz used to read the analog output of the inertial sensors. With differential corrections, GPS provides accurate position information that is not corrupted by the same bias and scale factor errors common in inertial sensors. Although corrupted by these terms, inertial sensors provide a much higher update rate more suitable for control. Combining these sensors together provides an estimate of the inertial sensor biases and then uses information from these sensors to fill in the gaps between GPS updates.

Because the filters used are purely kinematic, they do not rely on any vehicle model that might contain inaccuracy.

The "model" used is simply the relationships between acceleration, yaw rate and position for a rigid body, which only depends on the geometry of the measurement setup. This can be measured very accurately and does not change during operation. The GPS heading system allows the estimation problem to be separated into two Kalman filters instead of one extended Kalman filter. The traditional Kalman filter is comprised of a measurement update and a time update. Since the GPS measurements come in at a lower rate, the measurement update is only performed when GPS is available to estimate the sensor bias and zero out the state estimate error. The measurement update is described by:

$$x_+(t) = x_-(t) + K[y(t) - Cx_-(t)] \quad (31)$$

$$K = P_-(t)C^T[CP_-(t)C^T + R]^{-1} \quad (32)$$

$$P_+(t) = [I - KC]P_-(t) \quad (33)$$

where:

$x_-(t)$ = prior estimate of the system state at time t

$x_+(t)$ = updated estimate of the state at time t

$P_-(t)$ = prior error covariance matrix at time t

$P_+(t)$ = updated error covariance matrix at time t

K = Kalman gain

$y(t)$ = new measurement

C = observation matrix

R = measurement noise covariance

x represents the vehicle states of interest and y represents the measurements. Simple Euler integration of the inertial sensors is performed during the time update as described below.

$$x_-(t+1) = x_+(t) + \Delta t \dot{x}_+(t) \quad (34)$$

$$P_-(t+1) = A_d P_+(t) A_d^T + Q \quad (35)$$

where A_d represents the discretized dynamics and Q is the process noise covariance. This is the Kalman filter structure used to estimate the vehicle position, and heading, for implementation of the potential field controller.

The GPS receivers used to calculate the heading and position information have an inherent latency due to computation and data transfer delays. Therefore, the time tags in the GPS measurement and the synchronizing pulse per second (PPS) from the receiver are used to align the GPS information with the inertial sensor measurements. Upon a GPS measurement, the time tags are used to calculate the time to which the GPS measurement corresponds. The integrated inertial value at the identified time and the GPS value are used for the measurement update. From this measurement update, the accelerometer measurements are then used to integrate forward in time until the next GPS update becomes available. This synchronizing process is extremely important when

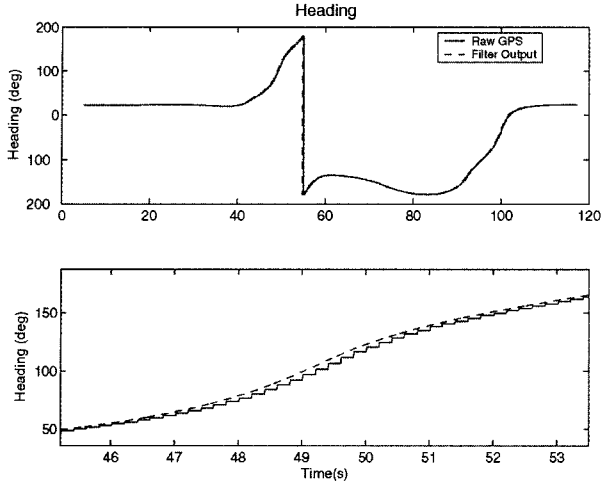


Figure 7. Heading: GPS and Kalman filter output.

trying to get real-time estimates of the vehicle states (Ryu, 2002).

6.2. Heading

For the heading Kalman filter, a linear dynamic system is constructed using the yaw rate as an input and the heading from a two-antenna GPS system for the measurement update.

$$\begin{bmatrix} \dot{\psi} \\ \dot{r}_{bias} \end{bmatrix} = \begin{bmatrix} 0 & -1 \\ 0 & 0 \end{bmatrix} \begin{bmatrix} \psi \\ r_{bias} \end{bmatrix} + \begin{bmatrix} 1 \\ 0 \end{bmatrix} r_m + \text{noise} \quad (36)$$

$$\psi_m^{GPS} = [1 \ 0] \begin{bmatrix} \psi \\ r_{bias} \end{bmatrix} + \text{noise} \quad (37)$$

where ψ is the heading, r_m is the measured yaw rate, r_{bias} is the yaw rate sensor bias, and ψ_m^{GPS} is the GPS heading from the two-antenna GPS system. Figure 7 shows the raw (unsynchronized in time) GPS measurement from the Beeline system along with the Kalman filter output. At the macro scale the two are indistinguishable. The bottom plot shows a zoomed in section of the heading. The Kalman filter output leads the GPS output as expected because of the latency in the GPS signal discussed earlier. The filter gives smooth heading information between GPS updates, ideal for high speed vehicle control.

6.3. Position

The position Kalman filter uses lateral and longitudinal accelerations along with DGPS position information to obtain a high update global position of the vehicle. For this Kalman filter the linear dynamic system uses the vehicle's lateral and longitudinal accelerations as inputs and the DGPS east and north positions for the measure-

ment update. The heading output of the first filter is used to transform the accelerations from body fixed to global coordinates.

$$\begin{bmatrix} \dot{P}_N \\ \ddot{P}_N \\ \dot{a}_{x \text{ bias}} \\ \dot{P}_E \\ \ddot{P}_E \\ \dot{a}_{y \text{ bias}} \end{bmatrix} = A \begin{bmatrix} P_N \\ \dot{P}_N \\ P_E \\ \dot{P}_E \\ a_{y \text{ bias}} \end{bmatrix} + B \begin{bmatrix} a_{xm} \\ a_{ym} \end{bmatrix} + \text{noise} \quad (38)$$

where p_N and P_E are the north and east position of the vehicle, respectively, $a_{x \text{ bias}}$ is the longitudinal accelerometer bias, $a_{y \text{ bias}}$ is the lateral accelerometer bias, a_{xm} is the measured longitudinal acceleration, and a_{ym} is the measured lateral acceleration. The matrices A and B are

$$A = \begin{bmatrix} 0 & 1 & 0 & 0 & 0 & 0 \\ 0 & 0 & -\cos \psi & 0 & 0 & \sin \psi \\ 0 & 0 & 0 & 0 & 0 & 0 \\ 0 & 0 & 0 & 0 & 1 & 0 \\ 0 & 0 & \sin \psi & 0 & 0 & \cos \psi \\ 0 & 0 & 0 & 0 & 0 & 0 \end{bmatrix} \quad (39)$$

$$B = \begin{bmatrix} 0 & 0 \\ \cos \psi & -\sin \psi \\ 0 & 0 \\ 0 & 0 \\ -\sin \psi & -\cos \psi \\ 0 & 0 \end{bmatrix} \quad (40)$$

with the heading, ψ , coming from the heading Kalman filter. The measurement update equation is

$$\begin{bmatrix} P_N^{GPS} \\ P_E^{GPS} \end{bmatrix} = \begin{bmatrix} 1 & 0 & 0 & 0 & 0 & 0 \\ 0 & 0 & 0 & 1 & 0 & 0 \end{bmatrix} \begin{bmatrix} P_N \\ \dot{P}_N \\ P_E \\ \dot{P}_E \\ a_{y \text{ bias}} \end{bmatrix} + \text{noise} \quad (41)$$

where P_N^{GPS} and P_E^{GPS} are the north and east position measurements from DGPS.

Figure 8 and 9 compare the east and north position from DGPS measurements with the Kalman filter output. Similar to the heading case the Kalman filter data fills in the gaps between the DGPS measurements providing a

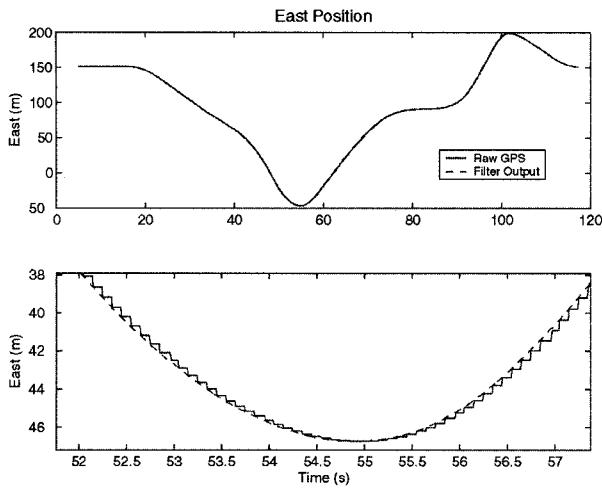


Figure 8. East position: raw GPS and Kalman filter output.

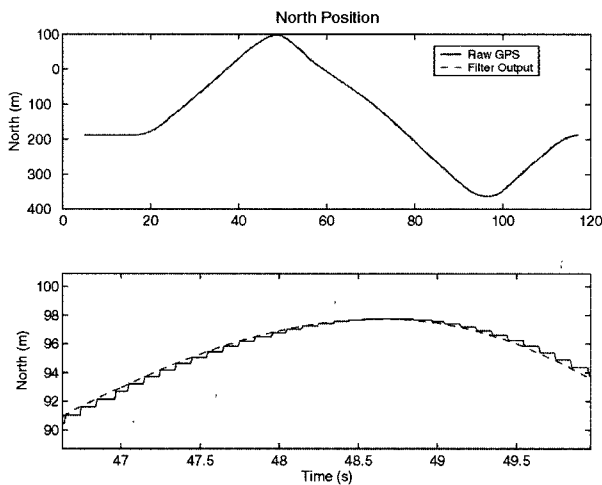


Figure 9. North position: Raw GPS and Kalman filter output.

smooth, clean signal.

The Kalman filter approach to GPS/INS integration proposed here is novel in that the output of the heading filter is used by the position filter. It is the use of a GPS heading system that allows this decoupling of the heading and position Kalman filters. This is not an extended Kalman filter, it is instead a combination of two ordinary Kalman filters and thus does not require linearization. With this structure the convergence properties of the filter setup are more intuitive, and the tuning of the filters can be performed independently.

7. PRECISION MAPS

7.1. Purpose

The combination of GPS and INS provides an accurate and high bandwidth measurement of global position and attitude. Lanekeeping assistance requires knowledge of the vehicle's deviation from the lane center. Using a digital road map, the vehicle's current position is used to calculate the lateral and heading error of the vehicle. Road maps are already available for virtually every road in the United States, but not with sufficient accuracy for lanekeeping. High precision maps will soon be available from commercial firms with the necessary accuracy for lanekeeping. Research is underway both in academia and industry on automated ways to generate high precision road maps. One approach by Rogers et al. is to create maps based on averaging the trajectories of many vehicles over the same stretch of road (Rogers, 1999). For the purposes of experimental validation of this lanekeeping system, maps are created manually for the specific test area needed.

7.2. Map Generation

The map making process consists of driving the road loop at constant speed and recording position measurements from DGPS. A smooth map is generated from this data using constrained least squares. This map consists of a predetermined number of segments, each of which is a parametric polynomial function of a distance parameter σ (Figure 10). The number of segments is chosen so that each segment will capture a feature of the road while the constant speed ensures that the density of data points is roughly uniform. For simplicity the segments contain equal numbers of data points. The polynomials describing each segment are given by

$$Y_i(\sigma) = a_{y_i}\sigma^3 + b_{y_i}\sigma^2 + c_{y_i}\sigma + d_{y_i} \quad (42)$$

$$X_i(\sigma) = a_{x_i}\sigma^3 + b_{x_i}\sigma^2 + c_{x_i}\sigma + d_{x_i} \quad (43)$$

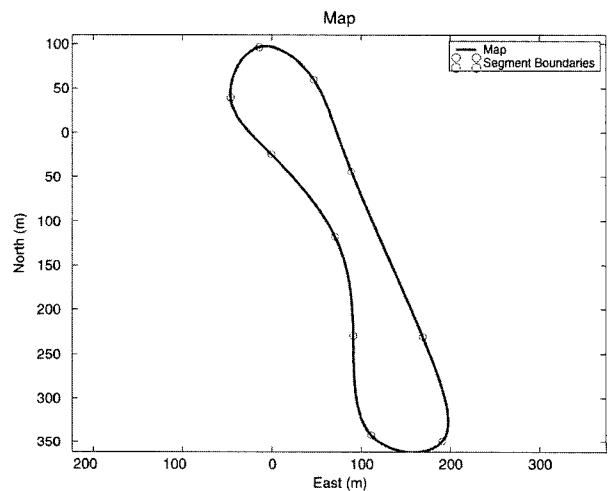


Figure 10. Map of lane center showing segment boundaries.

where a_{yi} and a_{xi} denote the i th coefficient in the polynomial for Y and X , and σ varies from 0 to 1 on each segment.

The determination of the polynomial coefficients is formed as a constrained least squares problem (Bjorck, 1996). To setup this problem, the unconstrained least squares solution is needed.

$$x_{in} = Hk_{xls} \quad (44)$$

$$y_{in} = Hk_{yls} \quad (45)$$

where k_{xls} and k_{yls} contain the best fit polynomial coefficients for all the segments.

$$k_{xls} = (a_{x1} \ b_{x1} \ c_{x1} \ d_{x1} \dots \ a_{xn} \ b_{xn} \ c_{xn} \ d_{xn})^T \quad (46)$$

$$k_{yls} = (a_{y1} \ b_{y1} \ c_{y1} \ d_{y1} \dots \ a_{yn} \ b_{yn} \ c_{yn} \ d_{yn})^T \quad (47)$$

$$H = \begin{pmatrix} \bar{\sigma}^3 & \bar{\sigma}^2 & \bar{\sigma} & 1 & 0 & 0 & 0 & 0 \dots \\ 0 & 0 & 0 & 0 & \bar{\sigma}^3 & \bar{\sigma}^2 & \bar{\sigma} & 1 \dots \\ \vdots & \vdots & \vdots & \vdots & \vdots & \vdots & \vdots & \ddots \end{pmatrix} \quad (48)$$

where $\bar{\sigma}$ denotes the entire σ vector, ranging from 0 to 1, of length equal to the number of data points in the segment. The unconstrained solution is then found as the least squares solution of the above, or

$$k_{yls} = (H^T H)^{-1} H^T y_{in} \quad (49)$$

$$k_{xls} = (H^T H)^{-1} H^T x_{in} \quad (50)$$

The standard least squares solution does not ensure that the map will be continuous or smooth at the segment boundaries.

For a useful map, we must require that it be continuous at segment ends, and that the slope be continuous at segment boundaries.

$$Y_i(1) = Y_{i+1}(0) \quad (51)$$

$$X_i(1) = X_{i+1}(0) \quad (52)$$

$$\frac{\partial Y_i}{\partial \sigma}(1) = \frac{\partial Y_{i+1}}{\partial \sigma}(0) \quad (53)$$

$$\frac{\partial X_i}{\partial \sigma}(1) = \frac{\partial X_{i+1}}{\partial \sigma}(0) \quad (54)$$

Thus, we must require that

$$a_{yi} + b_{yi} + c_{yi} + d_{yi} = d_{yi+1} \quad (55)$$

$$a_{xi} + b_{xi} + c_{xi} + d_{xi} = d_{xi+1} \quad (56)$$

$$3a_{yi} + 2b_{yi} + c_{yi} = c_{yi+1} \quad (57)$$

$$3a_{xi} + 2b_{xi} + c_{xi} = c_{xi+1} \quad (58)$$

Using these constraint equations, the problem can be reformulated as a constrained least squares problem in which these equality constraints are placed on the problem in the form of a matrix equation. This matrix

equation is not a minimization, but rather a series of equations that must be satisfied:

$$Ak_{xopt} = 0 \quad (59)$$

$$Ak_{yopt} = 0 \quad (60)$$

where the A matrix is formed to constrain the continuity and smoothness at segment boundaries.

In order to form a closed map, the last rows of the A matrix must enforce the continuity and smoothness between the final and first segments of the map, in the same way outlined above. With the problem formulated in this way, we can find the constrained least squares solution as

$$k_{yopt} = k_{yls} - (H^T H)^{-1} A^T [A(H^T H)^{-1} A^T]^{-1} A k_{yls} \quad (61)$$

$$k_{xopt} = k_{xls} - (H^T H)^{-1} A^T [A(H^T H)^{-1} A^T]^{-1} A k_{xls} \quad (62)$$

This approach provides a closed form solution for the map parameters from a given data set with an intuitive way to enforce constraints on the transition between segments.

7.3. Error Finding

For lanekeeping it is necessary to determine in real-time the lateral and heading deviation from the road map. The digital map gives the east and north position of the desired trajectory for some distance along the given map segment, σ , while the vehicle's east and north position is obtained from the Kalman filter output discussed in section 6. Assuming that the radius of curvature for each segment is large compared to the lateral deviation of the vehicle (as it is for highway lanekeeping), the shortest distance from the vehicle to the path is perpendicular with the path tangent. This is found by determining when the dot product between the vehicle's position relative to the map and the slope of the map is zero (Figure 11).

$$((X(\sigma) - P_E^{GPS}), (Y(\sigma) - P_N^{GPS})) \cdot (\dot{X}(\sigma), \dot{Y}(\sigma)) = 0 \quad (63)$$

If the polynomial used to make the map is of order, n , this dot product polynomial is order $2n-1$ and can be solved for the distance down the segment, σ_{veh} which corresponds to the point on the segment closest to the vehicle. Once

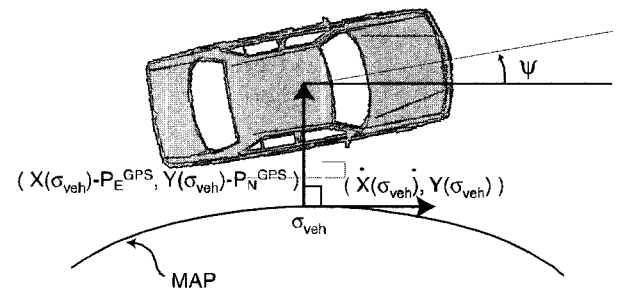


Figure 11. Error finding.

σ_{veh} is found that satisfies this equation it can be used to find the distance between the vehicle and the point on the path identified by σ_{veh} . Similarly, the heading error between the vehicle and the path can be found by comparing the heading from the Kalman filter output with the slope of the path at the point σ_{veh} . Since the point when the vehicle switches segments is unknown, the error finding algorithm assumes that the car is always moving forward and checks the segment from the previous solution along with the upcoming segment when solving for the lateral and heading errors.

7.4. Map Geometry

Using maps with segments of constant curvature can result in uncomfortable vehicle motion. Because the curvature is not continuous at segment boundaries, there is a discontinuity of slope of the heading error at segment boundaries. Although this does not cause a discontinuity of commanded steering position at the boundaries, it does cause a discontinuity of commanded steering rate. To remedy this problem, the map can be modified to constrain curvature to be constant at segment boundaries. This constraint can be easily added to the matrix A of Equations 59 and 60.

Roads are not constructed with continuous curvature. In most areas roads consist exclusively of straight segments and segments of constant curvature (Cal.DoT, 2001). Some areas allow segments of varying curvature (spirals) as connectors. It was originally assumed that the road map should exactly represent lane center, but initial driver feel tests show that the map should not have the same characteristics as the road. How to design a map to combine smooth movement of the vehicle and accurate representation of the road remains an open issue.

8. RESULTS AND SIMULATION

8.1. Test Setup

Experimental testing of the lanekeeping system was



Figure 12. Corvette test vehicle at Moffett field.

Table 1. Vehicle and road parameters.

Antenna locating behind C.G. (m)	0.7 m
m (kg)	1600
I_z (N/m ²)	2500
C_f (N/rad)	110000
C_r (N/rad)	100000
a (m)	1.3
b (m)	1.3
ρ_{max} (1/m)	1/25
$\dot{\rho}_{max}$ (1/ms)	0.01
$\ddot{\rho}_{max}$ (1/ms ²)	0

conducted on the West Ramp and West Parallel of Moffett Federal Airfield. Figure 12 shows the test vehicle at the Moffett Field test site. The map used for the experimental tests is given in Figure 10 along with the segment boundaries. Using this map and previous bounding results (Rossetter, 2003), the potential field gain is chosen so that the vehicle stays within 1m of the desired location given a speed of 12 m/s (25 mph). The pertinent vehicle, map, and controller parameters are given in Tables 1 and 2.

For the purposes of implementing the system, an accurate determination of the front cornering stiffness is needed to calculate the steering angle necessary for a given potential field control force as given in Equation (21). To compare experimental results to simulation, every one of the parameters in equations (12)~(14) is needed. Some of these can be directly measured, such as mass and distance from the center of gravity to each axle, while the cornering stiffnesses are estimated as in the reference by Ryu, *et al.* (2002). The yaw moment of inertia, I_z , is estimated to be the mass times the product of the distances from the CG to the axles. This approximation has been verified to be quite accurate for this test vehicle through comparison of data and simulation.

8.2. Lanekeeping Accuracy

Figure 13 shows the lateral error at the GPS antenna location (Table 1) of the vehicle for one loop around the map with no driver steering input. This is compared with a simulation using the simple vehicle model and the Corvette parameters from Table 1. The match between

Table 2. Controller and vehicle parameters.

	Figure 13	Figure 15
P.F gain k	15000	10000
x_{1a} (m)	7	10.5

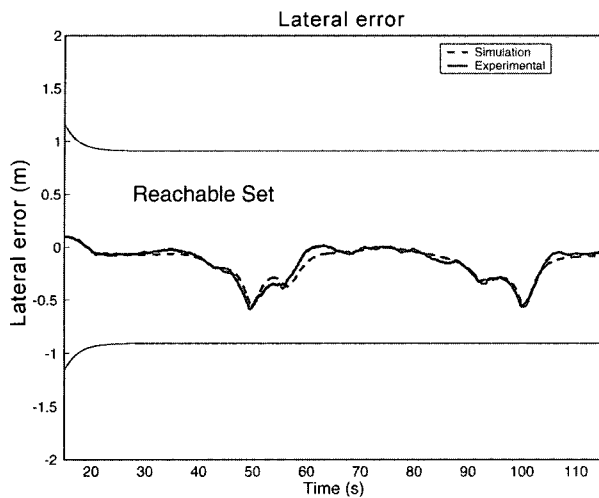


Figure 13. Lateral error: simulation vs. experiment with $k=15000$.

the two is quite remarkable with a peak difference of around 10 cm but much smaller errors for most of the run, as shown in Figure 14. The close match to simulation is impressive considering the simple model used as well as the absence of noise and steering dynamics in the simulation. The simulation does not take into account the surface of the testing area, which contained numerous pavement seams and rectangular holes for aircraft tie-downs.

From the highway design manual published by the California Department of Transportation (2001), a standard freeway lane is 3.6m, leaving 0.85m on each side of the 1.9m wide Chevrolet Corvette. The experimental results verify that the vehicle remains in the lane without driver steering commands, achieving a maximum lateral

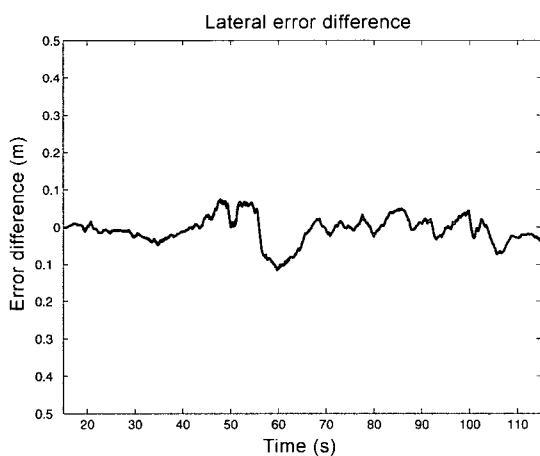


Figure 14. Difference in lateral error between simulation and experiment.

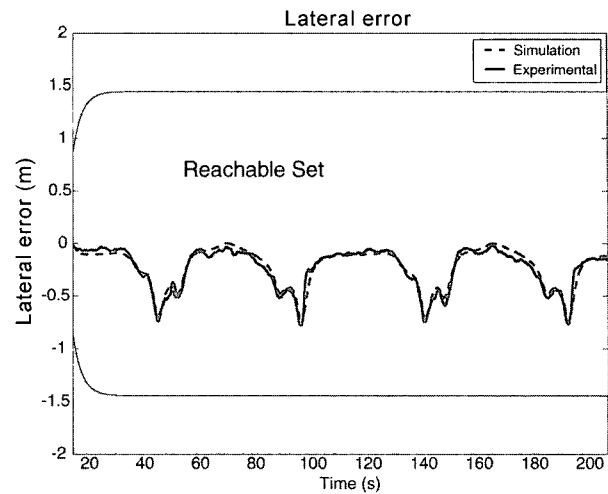


Figure 15. Lateral error with $k=10000$.

error of around 0.6m. The repeatability of the vehicle motion during cornering is significant because it creates a response that is easily predicted by the driver. There are no unexpected motions that might force the driver to make unnatural steering commands to remain on the path (i.e. the driver steering the wrong direction around a corner).

The simple simulation's close match to the experimental results gives great confidence in the bounds obtained in previous results. Figure 13 shows the lateral error from the experiment and simulation along with the bounds used for the potential field design. The unshaded region defines the reachable set for the vehicle's lateral position, which represents the maximum excursion from lane center for this vehicle at this speed on this map. The bound is somewhat conservative because it is based on the maximum geometric characteristics of the map, however it still provides a useful method to choose the gain of the potential field. This bounding technique is a powerful tool, providing a safety guarantee for the lanekeeping system.

Figure 10 shows the lateral error for a two-lap test run with a lower potential field gain. As expected the vehicle drifts further into the potential around each turn. The mathematical bound on the vehicle's motion also extends further as a result of the lower gain. This demonstrates how the potential field gain can be chosen to bound the motion of the vehicle within a lane. Again the simulation matches the experiment quite closely.

9. FUTURE DIRECTIONS

A successful driver assistance system has to increase the vehicle safety and be acceptable for the user. A natural direction for this work is to focus on driver acceptance

issues. One major area affecting driver comfort is the type of steering wheel feedback given to the user. With steer-by-wire, there is a wealth of options for the type of feedback used. Forces can be added based on the vehicle states, the position in the potential, as well as the states of the steering wheel itself. Incorporating force feedback requires actuation at the steering wheel. Since the steering wheel controls part of the overall steering command, the stability of the lanekeeping system will be altered. When designing a force feedback system, the stability conditions for the overall system must be considered, in a variety of situations. With the driver steering normally the feedback should feel intuitive to the driver. With hands off the steering wheel, the system must still be stable and maintain the vehicle within the lane. Another intriguing avenue of study is the stability of the system with the user in the loop. For example, if there is sufficient delay in the feedback system, the driver may not be able to stabilize the vehicle.

10. CONCLUSION

This successful experimental implementation of the potential field lanekeeping assistance system shows excellent lanekeeping performance and a close match to simulation. The test setup uses a novel GPS/INS configuration including a GPS heading system, which allows the estimation problem to be decoupled into two ordinary Kalman filters. The combination of this estimation technique with polynomial lane maps provides smooth and comfortable lanekeeping assistance. The success of these experiments confirms that the system can be used to avoid lane excursions in the absence of driver inputs and can be designed using theoretical performance guarantees. These results also underscore the importance of driver feel in a system such as this.

ACKNOWLEDGEMENT—The authors would like to thank Michael Grimaldi, Robert Wiltse and Pamela Kneeland at General Motors Corporation for the donation of the Corvette and the GM Foundation for the grant enabling its conversion to steer-by-wire. The authors would also like to thank Dr. Skip Fletcher, T.J. Forsyth, Geary Tiffany and Dave Brown at the NASA Ames Research Center for the use of Moffett Federal Airfield. This material is based upon work supported by the National Science Foundation under Grant No. CMS-0134637 with additional support from a National Science Foundation Graduate Research Fellowship.

REFERENCES

- Ake, B. (1996). *Numerical Methods for Least Squares Problems*. SIAM. Philadelphia. PA.
- California Department of Transportation (2001). The Highway Design Manual.
- Crow, S. C. and Manning, F. L. (1992). Differential GPS control of starcar 2. *Journal of the Institute of Navigation* **39**, Winter. 383–405.
- Farrell, J. and Barth, M. (2000). Integration of GPS-aided INS into AVCSS. *Technical Report MOU 374*, California PATH Program.
- Fuhrer, T., Dilger, E. and Muller, B. (1998). Distributed fault tolerant and safety critical applications in vehicles—a time triggered approach. In *Proceedings of the 17th International Conference on Computer Safety, Reliability and Security*, Heidelberg, Germany.
- Fujioka, T., Shirano, Y. and Matsushita, A. (1999). Driver's behavior under steering assist control system. In *Proceedings of IEEE Intelligent Transportation Systems*, 246–251.
- Gehrig, S. K., Gern, A., Heinrich, S. and Woltermann, B. (2002). Lane recognition on poorly structured roads—the bots dot problem in California. In *Proceedings of the IEEE Intelligent Transportation Systems*, 67–71.
- Gerdes, J. C. and Rossetter, E. J. (2001). A unified approach to driver assistance systems based on artificial potential fields. *ASME Journal of Dynamic Systems, Measurement, and Control* **123**, September. 431–438.
- Han-Shue Tan, B. Bougler and Zhang, W.-B. (2002). Automatic steering based on roadway markers: from highway driving to precision docking. *ASME Journal of Dynamic Systems, Measurement, and Control* **37**, May. 315–338.
- Hedenetz, B. (1998). A development framework for ultra-dependable automotive systems based on a time-triggered architecture. In *Proceedings of the Real-Time Systems Symposium*, Madrid, Spain.
- Hogan, N. (1985). Impedance control: An approach to manipulation. parts I-III. *ASME Journal of Dynamic Systems, Measurement, and Control* **107**, 1–24, March.
- Khatib, O. (1986). Real-time obstacle avoidance for manipulators and mobile robots. *International Journal of Robotics Research* **5**, 1, 90–98.
- LeBlanc, D. J., Venhovens, P. J., Lin, C.-F., Pilutti, T. E., Ervin, R. D., Ulsoy, A. G., MacAdam, C. and Johnson, G. E. (1996). Warning and intervention system to prevent road-departure accidents. *Vehicle System Dynamics* **25**, 383–396.
- NHTSA. *Traffic Safety Facts 2001 (2002)*. Technical report, National Highway Traffic Safety Administration.
- Omae, M. and Fujioka, T. (1999). DGPS-based position measurement and steering control for automatic driving. In *Proceedings of the American Control Conference*.
- Peng, H. and Tomizuka, M. (1993). Preview control for vehicle lateral guidance in highway automation. *ASME Journal of Dynamic Systems, Measurement, and Control* **115**, December. 679–686.
- Rech, B., Binfet-Kull, M. and Meyna, A. (2001).

- Definition of safety/reliability requirements for components of an electronic vehicle system such as steer by wire. In *Proceedings of the 4th European Conference and Exhibition on Vehicle Electronic Systems*, Coventry, UK.
- Regruto, D., Cerone, V. and Chinu, A. (2002). Experimental results in vision-based lane keeping for highway vehicles. In *Proceedings of the 2002 American Control Conference (ACC)*, Anchorage, AK.
- Rekow, A., Bell, T., Bevely, D. and Parkinson, B. (1999). System identification and adaptive steering of tractors utilizing differential global positioning system. *Journal of Guidance, Control, and Dynamics* **22**, 671–674, Sept.-Oct..
- Rogers, S. (2000). Mining GPS data to augment road models. In *IEEE Conference on Intelligent Transportation Systems*.
- Rogers, S., Langley, P. and Wilson, C. (1999). Mining GPS data to augment road models. In *International Conference on Knowledge Discovery and Data Mining*.
- Rossetter, E. J. (2003). A potential field framework for active vehicle lanekeeping assistance. *Ph.D Thesis*, Stanford University.
- Rossetter, E. J. and Gerdes, J. C. (2002). A study of lateral vehicle control under a ‘Virtual’ force framework. In *Proceedings of the International Symposium on Advanced Vehicle Control (AVEC)*.
- Rossetter, E. J. and Gerdes, J. C. (2003). Safety guarantees for lanekeeping assistance systems with time-varying disturbances: A Lyapunov approach. In *Proceedings of the ASME International Mechanical Engineering Congress and Exposition*.
- Ryu, J., Rossetter, E. J. and Gerdes, J. C. (2002). Vehicle sideslip and roll parameter estimation using GPS. In *Proceedings of the International Symposium on Advanced Vehicle Control (AVEC)*.
- Schiller, B., Morellas, V. and Donath, M. (1998). Collision avoidance for highway vehicles using the virtual bumper controller. In *Proceedings of the IEEE International Symposium on Intelligent Vehicles*.
- USCG. Nationwide dgps status report (2003). *Technical report*, U.S. Coast Guard Navigation Center, January.
- Yih, P., Ryu, J. and Gerdes, J. C. (2003). Modification of vehicle handling characteristics via steer-by-wire. In *Proceedings of the American Control Conference*.